Symbiotic *Lactobacillus brevis* promote stem cell expansion and tumorigenesis in the *Drosophila* intestine

Meghan Ferguson[1,2], Kristina Petkau[1], Minjeong Shin[1], Anthony Galenza[1], David Fast[1], and Edan Foley[1,2]*.

1: Department of Medical Microbiology and Immunology, Faculty of Medicine and Dentistry, University of Alberta, Edmonton, AB, Canada

2: Department of Cell Biology, Faculty of Medicine and Dentistry, University of Alberta, Edmonton, AB, Canada

*Corresponding Author: Edan Foley efoley@ualberta.ca

SUMMARY

Commensal bacteria regulate the growth and differentiation of intestinal epithelial cells. Deregulated growth compromises the efficacy of critical repair pathways, and promotes tissue dysplasia and tumorigenesis. Despite the importance of bacteria-derived cues for tissue homeostasis, we know little about how intestinal commensals directly influence stem cell division programs. In this study, we examined the effects of common fly symbionts on tissue growth and tumorigenesis in the *Drosophila* intestine. We identified the cell wall of *Lactobacillus brevis* as a potent stimulator of Notch-deficient tumor growth. Our work uncovered a complex feed-forward loop between tumor growth and intestinal colonization by *L. brevis*. Mechanistically, we showed that *L. brevis* disrupts the expression and apicobasal distribution of integrins in intestinal progenitors, and supports an increase in stem cell numbers characterized by elevated numbers of symmetric stem cell divisions. Collectively, this work highlights host-commensal interactions that influence intestinal growth and stem cell division.

INTRODUCTION

Commensal bacteria interact with the intestine to influence immunity, metabolism and growth. For instance, the microbiome promotes intestinal growth in model organisms as diverse as flies, fish and rodents (Buchon *et al*., 2009; Broderick *et al*. 2014; Cheesman *et al*., 2011; Zackular *et al*., 2013; Li *et al*., 2012), and disruptions to microbial diversity in the intestine is associated with proliferative diseases of the intestine, such as colorectal cancer in humans (Gagnière *et al*., 2016; Zeller *et al*., 2014). Intestinal growth is dictated by the actions of multipotent intestinal stem cells (ISCs) (Jiang and Edgar, 2011; Micchelli and Perrimon, 2006; Ohlstein and Spradling, 2006). Specifically, division and differentiation of ISCs are required for homeostatic epithelial renewal, and bursts of growth in response to tissue injury (Amcheslavsky et al., 2009; Biteau and Jasper, 2011; Buchon et al., 2009b; Jiang et al., 2009; Shaw et al., 2010). However, deregulated ISC division contributes to tissue overgrowth and oncogenesis (Cordero *et al*., 2012; Guo *et al*., 2013; Patel *et al*., 2015). Despite the importance of microbial cues for intestinal growth, we do not fully understand how commensal species influence the division of ISCs.

Drosophila is a popular model system to study host-commensal interactions due to an extensive genetic toolkit, and a simple, cultivatable microbiome that is easy to manipulate (Broderick and Lemaitre, 2012; Koyle *et al*., 2016). Additionally, the mechanisms that govern ISC division are evolutionarily conserved between flies and vertebrates (Miguel-Aliaga *et al*., 2018). For example, vertebrate and fly ISCs reside within a niche that provides homologous molecular cues to direct division and differentiation (Jiang and Edgar, 2011; Morrison and Spradling, 2008; Takashima and Hartenstein, 2012). Within this niche, integrins adhere ISCs to the basal extracellular matrix, direct cell polarity, align the mitotic spindle, and ensure the proper localization of cell fate determinants required for cell division (Chen *et al.*, 2018; Goulas *et al*., 2012). The majority of intestinal divisions occur asymmetrically to generate a daughter stem cell that remains within the niche, and a post-mitotic enteroblast that exits the niche and terminally

differentiates into a mature epithelial cell (Martin *et al.*, 2018; Micchelli and Perrimon, 2006; Ohlstein and Spradling, 2006, 2007). However, in contrast to other stem cells, such as germline stem cells, ISCs are not committed to asymmetric divisions. Approximately 20% of ISC divisions are symmetric, generating either enteroblast pairs, or ISC pairs (Hu and Jasper, 2019; Jin et al., 2017; O'Brien et al., 2011). Over time, this pattern of symmetric growth results in the expansion, or disappearance, of individual stem cell lineages, generating clonal stem cell populations across the epithelium (de Navascués *et al*., 2012). In flies, integrins are required for ISC maintenance and depletion of integrins increases the number of symmetric divisions, expanding stem cell populations, and causing intestinal hyperplasia (Goulas *et al.*, 2012; Lin *et al*., 2013; Okumura *et al*., 2014). Importantly, relationships between integrins and progenitor cell growth appear to be evolutionarily conserved, as integrin loss also causes intestinal hyperplasia in mice (Jones *et al.*, 2006).

Subsequent differentiation of enteroblasts is determined by the activity of the Notch signaling pathway. In response to high Notch activity, enteroblasts differentiate as large, absorptive enterocytes, while low Notch activity instructs enteroblasts to differentiate into secretory enteroendocrine cells (Biteau and Jasper, 2014; Guo and Ohlstein, 2015; Ohlstein and Spradling, 2007; Zeng and Hou, 2015). Loss of Notch activity in the progenitor compartment leads to the rapid growth of multilayered tumors populated by hyperplastic progenitors, and an accumulation of secretory enteroendocrine cells (Patel *et al.*, 2015). Disruptions to Notch signaling causes similar dysplastic phenotypes in fish and mice (Crosnier *et al*., 2005; Qiao and Wong, 2009), and the spontaneous accumulation of mutations at the Notch locus is linked to the age-dependent development of intestinal tumors in adult *Drosophila* (Siudeja *et al.*, 2015). We previously showed that the bacterial microbiome promotes the growth of Notch-deficient tumors in the fly midgut (Petkau *et al*., 2017). However, it is unclear which commensal bacteria promote tumorigenesis, and how this happens. In this study, we monitored tumor growth in response to common

fly symbionts, and determined the impacts of those bacteria on ISCs. We found that the cell wall of *Lactobacillus brevis* accelerated the growth of Notch-deficient tumors. Interestingly, tumor growth promoted the ingestion of live bacteria, and dampened intestinal immune defenses, leading to an accumulation of *L. brevis* within the intestine. Mechanistically, we found that *L. brevis* decreased the expression, and altered the apicobasal localization, of integrins in intestinal progenitors. In line with effects of integrins on stem cell divisions, we found that *L. brevis* promoted an expansion of the stem cell pool by increasing the frequency of symmetric stem cell divisions. In combination, these data detail a feed-forward loop between a common fly symbiont and the expansion of mutant stem cells in the fly midgut.

RESULTS

L. brevis promotes tumor growth in the *Drosophila* intestine.

To generate intestinal tumors, we disrupted Notch signaling specifically in ISCs and enteroblasts (collectively referred to as progenitor cells) using a temperature-inducible escargot gene driver (esg^{ts}). Depletion of *Notch* from intestinal progenitors (esg^{ts}/N^{RNAi}) in adult females resulted in multilayered tumors populated by progenitors marked by GFP and enteroendocrine cells marked by Prospero (Pros) (Suppl. Fig. 1A-C) as previously described (Patel *et al*., 2015). To identify bacterial species that drive tumorigenesis, we examined the posterior midguts of gnotobiotic adult esg^{ts}/N^{RNAi} flies that we associated exclusively with common species of *Drosophila Lactobacillus* symbionts, a dominant genus within the fly microbiome (Adair *et al*., 2018). To focus exclusively on tumor growth in the adult, we raised esg^{ts}/N^{RNAi} larvae with a conventional microbiome under temperature conditions that prevent Notch inactivation. Upon eclosion, we fed adult flies an antibiotic cocktail that removes the bacterial microbiome, and then re-associated the fly with the *Lactobacillus* symbionts, *Lactobacillus brevis* (*Lb*), or *Lactobacillus plantarum* (*Lp*) (Fig. 1A). We compared the effects of each mono-association on the growth of Notch-deficient tumors to conventionally reared (CR) esg^{ts}/N^{RNAi} flies with a polymicrobial gut microbiota. In line with previous data, we observed widespread distribution of tumors in CR intestines after 5 days of Notch-depletion compared to wild-type controls (Fig. 1B-C). Conversely, germ-free (GF) intestines visibly lacked Notch-deficient tumors and more closely resemble wild-type intestines (Fig. 1D). We also observed substantial differences in tumor size and frequency between flies that we associated with *Lb* or *Lp*. Association with *Lp* phenocopied GF flies, yielding intestines that typically lacked tumors (Fig. 1E). In contrast, *Lb* promoted extensive tumor growth throughout the posterior midgut (Fig. 1F), suggesting that *Lb* is sufficient to drive the growth of Notch-deficient tumors. To accurately measure the impact of bacterial association on tumor growth, we developed a four-point system to quantify tumor

incidence, where level IV intestines contain both progenitor and enteroendocrine cell tumors (Fig. 1G). In a blinded assay, we found that 85% of CR intestines contained level IV tumors, while only 20% of GF intestines had level IV tumors upon depletion of *Notch* from progenitor cells (Fig. 1G). Consistent with our initial observations, we found that tumor incidence was indistinguishable between GF intestines, and *Lp*-associated intestines (Fig. 1H). In contrast, *Lb* enhanced tumor incidence to the point where 100% of intestines had level IV tumors within five days of Notch inactivation. To measure tumor burden in the respective treatment groups, we quantified the proportion of the intestinal area occupied by progenitors and enteroendocrine cells in the respective intestines. Here, *Lb* significantly increased tumor burden compared to the intestines of CR, GF or *Lp* mono-associated flies (Fig. 1I), confirming an effect of *Lb*-association on the growth of intestinal tumors. We then asked which *Lb* factors support tumor growth. In our initial experiments, we found that GF flies fed heat-killed *Lb* has similar levels of tumor incidence and burden as intestines colonized by live *Lb* (Fig. 1J-K). Upon bacterial fractionation, we found that GF flies fed *Lb* cell wall extract also had the same level of tumor size and incidence as GF flies fed dead *Lb* (Fig. 1 L-M). Collectively, these data implicate *Lb* in the activation of progenitor growth programs, and indicate that cell wall components of *Lb* accelerate Notch-deficient tumor growth in the *Drosophila* midgut.

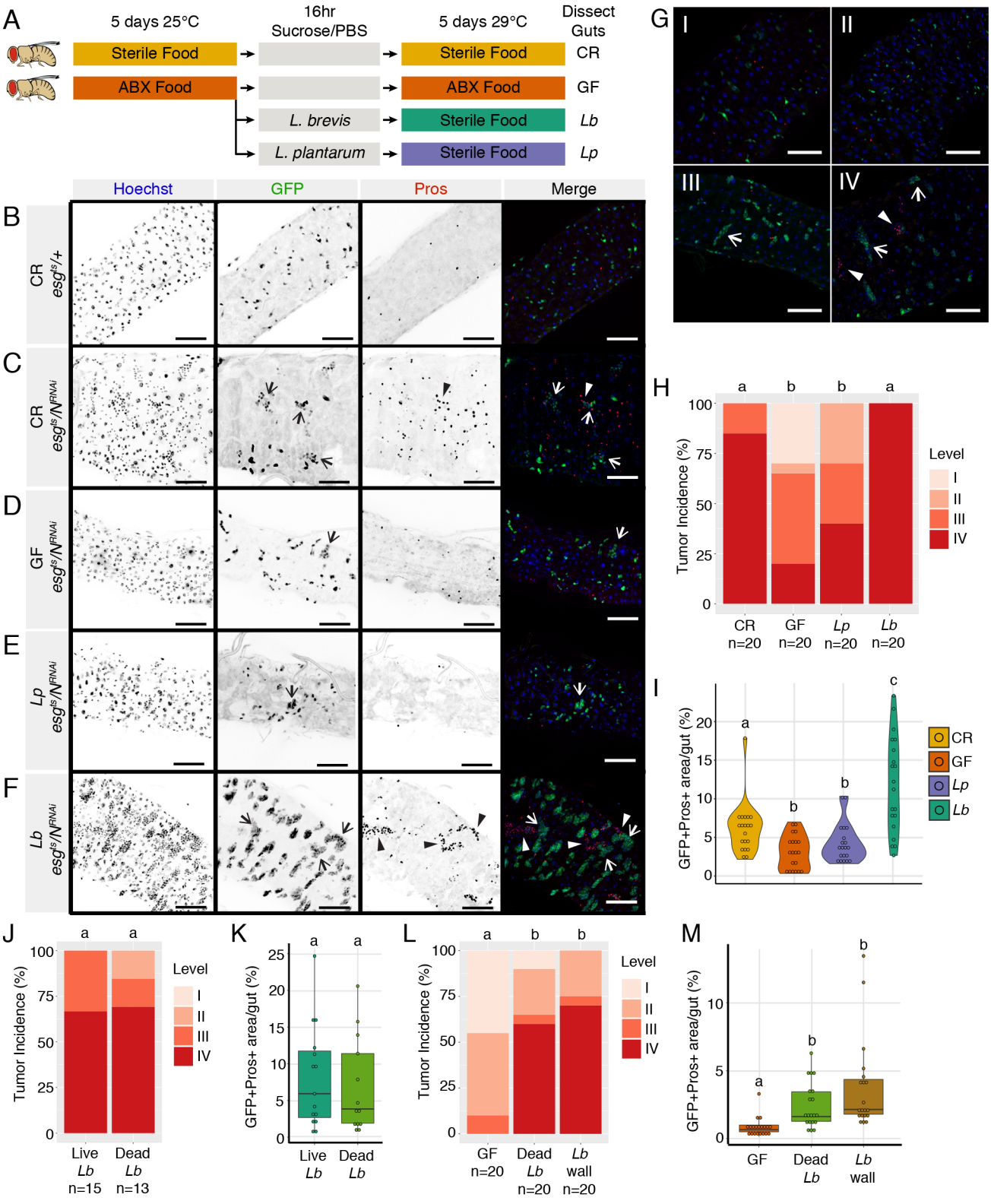

Figure 1. *L. brevis* promotes tumor growth in the *Drosophila* intestine. (A) Scheme for generating GF and gnotobiotic flies alongside CR controls. **(B)** Images of wild-type CR *esg^{ts}/+* intestines **(C-F)** Images of

esg^{ts}/N^{RNAi} posterior midguts 5 days after *Notch* knockdown and microbial manipulation. Hoechst marks DNA, GFP marks progenitor cells and Pros marks enteroendocrine cells. Level III tumours (open arrowheads) and level IV tumours (closed arrowheads). Scale bars = 50μm. **(G)** Tumor incidence grading system. I – healthy intestine, II – intestinal dysplasia without tumorigenesis, III – tumors populated by progenitors, IV – tumors populated by progenitors and enteroendocrine cells. **(H-M)** Tumor incidence and burden in gnotobiotic flies upon 5 days of *Notch* depletion. **(G-H)** Effects of *Lb* compared to CR, GF, and *Lp* monoassociated flies. **(I-J)** Effects of live *Lb* compared to GF flies fed dead *Lb*. **(K-L)** GF flies compared to GF flies fed either dead *Lb* or *Lb* cell wall extract. For all analyses, letters denote p<0.01. **(H,J,L)** Pairwise Wilcoxon tests. **(G,I,K)** Chi-squared test.

Notch inactivation disrupts antibacterial defenses in the host.

As *Lb* promotes the growth of intestinal tumors, we asked how progenitor cells respond to *Lb* colonization. To answer this question, we used RNA-Sequencing to determine the transcriptional profile of FACS-purified, GFP-positive progenitors in wild-type *esg^{ts}/+* and tumor-prone *esg^{ts}/N^{RNAi}* intestines colonized by *Lb* (Fig. 2A). As controls, we sequenced the transcriptomes of progenitors purified from GF flies, or flies mono-associated with *Lp*, a different *Lactobacillus* symbiont that does not stimulate growth. Importantly, our transcriptomic data for *esg^{ts}/N^{RNAi}* progenitors significantly overlapped with those obtained in a separate study (Patel et al., 2015). Principal Component Analysis (PCA) of our entire dataset revealed that progenitors from Notch-deficient intestines segregate from wild-type progenitors along PC1, independent of microbial association (Fig. 2B). Upon differential expression analysis, we found that the majority of genes altered upon Notch-depletion were common between GF, *Lb* and *Lp* intestines (Fig. 2C). GO term analysis of the core Notch-deficient response revealed a significant upregulation of biological processes involved in mitosis (Fig. 2D), including increased expression of cell cycle regulators,

and diminished expression of multiple *Enhancer of split (E(spl))* complex genes, downstream targets of the Notch pathway (Fig. 2E). In addition to the anticipated effects on growth and differentiation, we noticed an unexpected downregulation of immune processes in progenitors that lacked *Notch* (Fig. 2D). Specifically, the expression of genes that function within the antibacterial Immune deficiency (IMD) and Toll pathways were decreased in Notch-deficient progenitors (Fig. 2E). Deregulated expression of immune response genes is not secondary to the development of intestinal tumors, as we saw similar changes in the intestines of GF, and *Lp*-associated flies. These data suggest a genetic link between Notch signaling and antibacterial response pathways such as IMD. Consistent with putative links between Notch and immune pathway activity, earlier studies showed that mutation or constitutive activation of IMD alters the expression of Notch pathway genes in the fly intestine (Broderick et al., 2014; Petkau et al., 2017). Combined, these results indicate that depletion of *Notch* from intestinal progenitors promotes growth, and suppresses antibacterial defenses, independent of the microbiome.

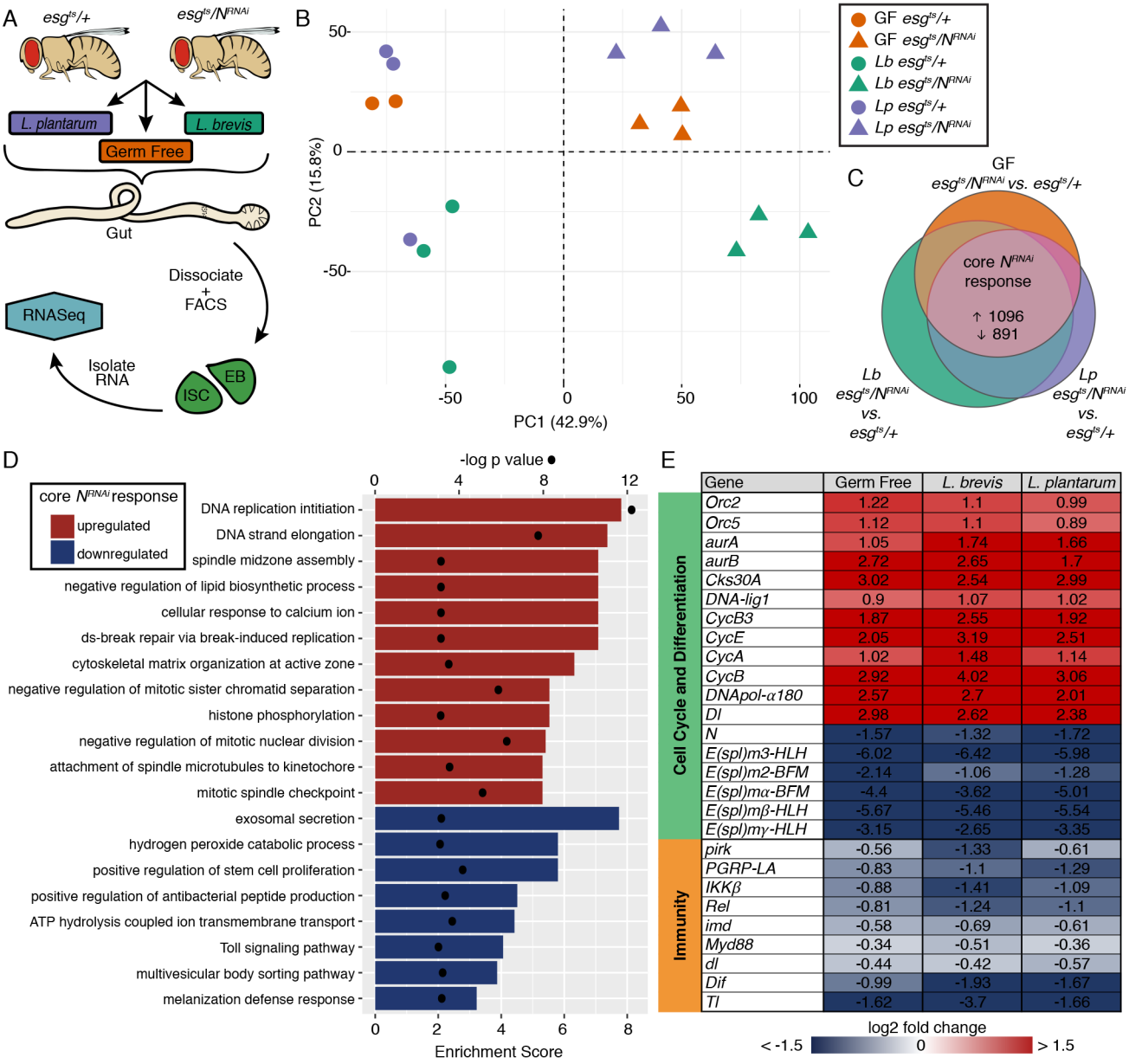

Figure 2. Notch inactivation disrupts antibacterial defenses in the host. (A) Workflow for the RNA-Seq of intestinal progenitors upon *Notch* knockdown and *Lb* colonization. **(B)** PCA plot from RNA-Seq project. Circles represent $esg^{ts}/+$ and triangles represent esg^{ts}/N^{RNAi} replicates. Different colors represent GF (orange), *Lb* (teal) or *Lp* (purple). **(C)** Genes altered by *Notch* knockdown (p<0.01, FDR <5%) in each microbial context showing the core response to knockdown of *Notch*. **(D)** Biological process GO terms enriched in the core *Notch* response. Enrichment score shown as bars and p values shown as dots. **(E)**

Log2 fold change of core *Notch* response genes (p<0.01, FDR <5%) involved in cell cycle/differentiation and immunity. Each column is a direct comparison of esg^{ts}/N^{RNAi} to $esg^{ts}/+$ under GF, *Lb* or *Lp* conditions.

Notch-deficiency promotes intestinal *L. brevis* overgrowth.

As loss of *Notch* from progenitors affects expression of immunity genes, we asked if disruptions to the Notch pathway influence bacterial abundance in the intestine. To answer this question, we completed a longitudinal measurement of bacterial load in the intestines of esg^{ts}/N^{RNAi} flies that we mono-associated with *Lb* or *Lp*. In general, our data agree with earlier reports that the total number of intestinal bacteria increase in flies with age (Clark *et al*., 2015; Guo *et al*., 2014). However, we also found that inactivation of the Notch pathway significantly increased the abundance of *Lb* and *Lp* at all times measured (Fig. 3A). For example, five-day-old esg^{ts}/N^{RNAi} flies have approximately 300 fold greater amounts of *Lb* than age-matched $esg^{ts}/+$ controls. We noticed similar effects of *Notch* depletion on *Lp* levels, suggesting that Notch-deficient intestines are compromised in their ability to prevent the expansion of symbiotic *Lactobacillus* species. Importantly, *Lb* and *Lp* increase to similar levels after 5 days of Notch inactivation, indicating that the ability of *Lb* to promote tumor growth is not merely a consequence of increased loads of intestinal *Lb*.

As Notch deficiency disrupts IMD activity, and results in *Lb* expansion, we asked if the IMD pathway directly influences *Lb* abundance in the intestine. To answer this question, we modulated IMD activity in *Lb* mono-associated flies, and measured intestinal bacterial load over time. Consistent with roles for IMD in the control of intestinal bacteria, we found that the intestines of *imd* mutant flies had significantly higher *Lb* loads than wild-type controls after five and ten days of bacterial colonization (Fig. 3B). Conversely, activation of the IMD pathway through expression of a constitutively active IMD in enterocytes ($Myo1A^{ts}$/*ImdCA*) for ten days reduced *Lb* load to approximately 4% of that found in *imd*

mutants. We noticed that the increased bacterial abundance in *imd* mutants was less pronounced than the increases observed upon *Notch* depletion in progenitors, suggesting that IMD-independent mechanisms contribute to the elevated bacterial numbers observed in esg^{ts}/N^{RNAi} intestines. Since bacterial presence in the gut requires consumption of bacteria-laden food (Blum et al., 2013; Pais et al., 2018), we tested the hypothesis that inactivation of Notch may also increase food consumption. Specifically, we monitored the feeding behaviour of starved $esg^{ts}/+$ and esg^{ts}/N^{RNAi} flies that were raised under CR, or GF conditions, or after mono-association with *Lb* or *Lp*. In each case, we found that flies with *Notch*-deficient progenitors consumed more food than their wild-type controls (Fig. 3C). These results indicate that *Notch* knockdown increases bacterial consumption, and compromises intestinal immune activity, favouring an increase in the levels of gut-associated *Lb*.

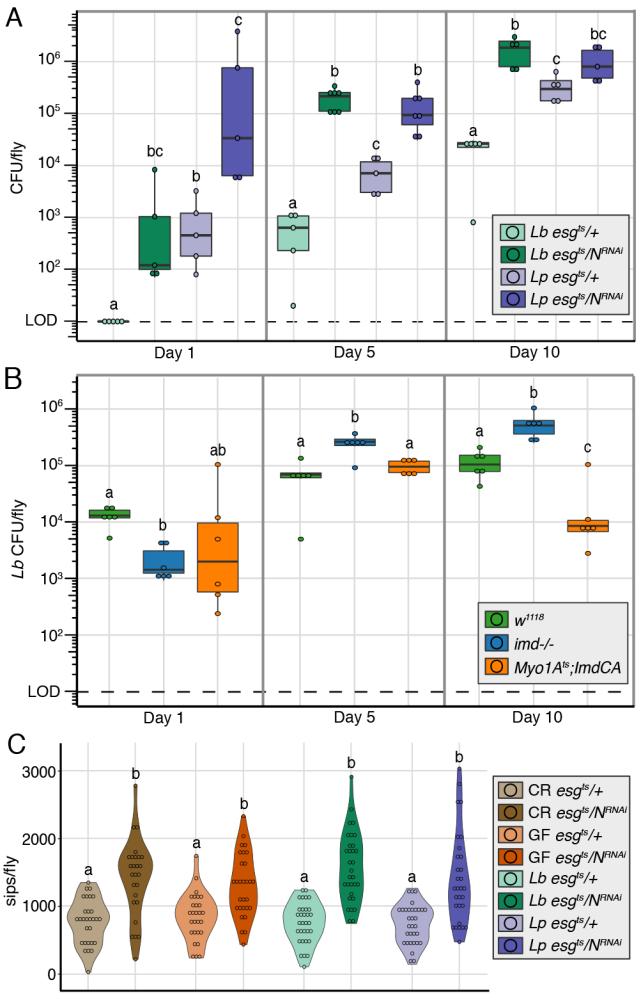

Figure 3. Notch-deficiency promotes intestinal *L. brevis* overgrowth. (A) Colony forming units (CFU) of *Lb* (green) and *Lp* (purple) per fly intestine over time in monoassociated $esg^{ts}/+$ and esg^{ts}/N^{RNAi}. Days are after transgene expression/bacterial colonization. **(B)** CFU of *Lb* per fly intestine over time in monoassociated wild-type (w^{1118}), *imd-/-*, and $Myo1A^{ts}$;*ImdCA*. For A and B, letters denote p<0.05 by pairwise Wilcoxon tests. LOD = limit of detection. **(C)** Effects of *Notch*-depletion on feeding behaviour (total sips/fly) in CR, GF, *Lb* and *Lp* $esg^{ts}/+$ and esg^{ts}/N^{RNAi} flies. For A-C, letters denote p<0.01 ANOVA followed by Tukey test.

***L. brevis* disrupts expression of integrins in progenitor cells.**

The data above describe a detrimental feed-forward loop between intestinal colonization by *Lb*, and the growth of Notch-deficient tumors. However, these data do not explain how *Lb* affects ISC growth within the intestine. To address this question, we identified transcriptional events in intestinal progenitors that were unique to association with *Lb* (Fig. 2B). We found that *Lb* induced a robust transcriptional response in comparison with GF flies in both wild-type and *Notch*-deficient progenitors, while *Lp* had comparatively moderate effects on gene expression (suppl. Fig. 2A,B). Specifically, *Lb* increased the expression of genes involved in fundamental stem cell processes, such as DNA replication, and mitotic spindle organization (Fig. 4A), as well as prominent cell cycle and growth regulators (Fig. 4B). Additionally, we noticed a striking *Lb*-dependent downregulation of genes involved in cell-cell adhesion, cell-matrix adhesion and cell polarity (Fig. 4A), particularly for genes that encode integrin complex proteins (Suppl. Fig. 2C). For example, association with *Lb* led to diminished expression of the fly integrins *myospheroid* (*mys*) and *scab*, the talin ortholog, *rhea*, and the integrin extracellular matrix ligand, *LanA* (Fig. 4B). The effects of *Lb* on the expression of genes associated with stem cell division and adhesion

are independent of host genotype, as we noticed similar phenotypes in the progenitors of *Lb*-associated $esg^{ts}/+$ and esg^{ts}/N^{RNAi} flies (Fig. 4B).

As *Lb* stimulates tumor growth and affects transcriptional growth programs in $esg^{ts}/+$ and esg^{ts}/N^{RNAi}, we asked if association with *Lb* also activates growth in wild-type progenitors. To answer this question, we mono-associated GF wild-type ($esg^{ts}/+$) flies with *Lb* and quantified phospho-histone 3 (PH3+) mitotic cells in the adult midgut. Similar to the effects of *Lb* on tumor growth, we found that *Lb* stimulates progenitor growth to significantly higher levels than those observed in CR, GF, or *Lp*-mono-associated intestines (Fig. 4C). Together, these data indicate that *Lb* promotes intestinal growth and blocks the expression of integrins in both wild-type and Notch-deficient progenitors.

A

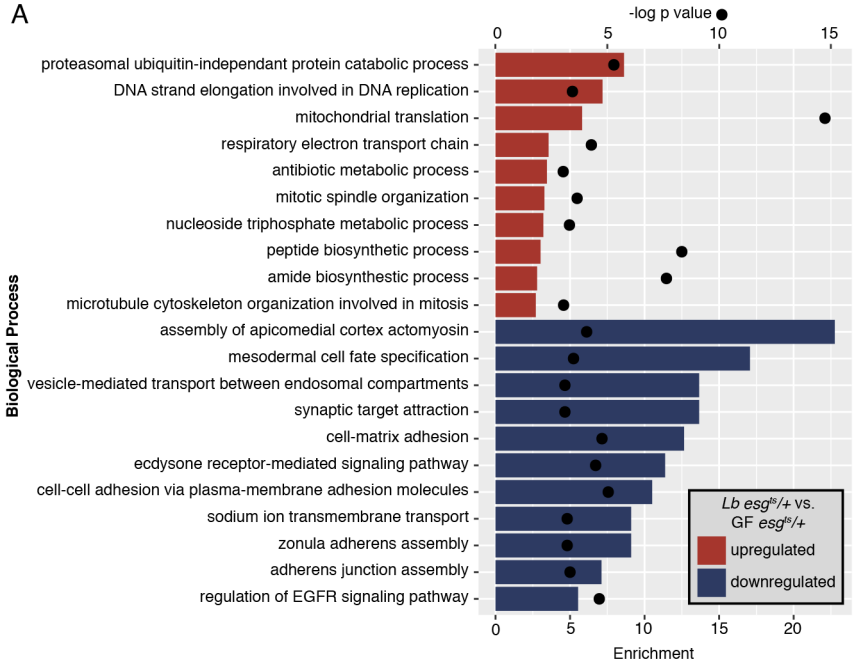

B

	Gene	Function	*L. brevis* compared to Germ Free		*L. brevis* compared to *L. plantarum*	
			esg^{ts}/+	esg^{ts}/N^{RNAi}	esg^{ts}/+	esg^{ts}/N^{RNAi}
Cell Adhesion/Polarity	*rhea*	Integrin adapter	-0.43	**-0.47**	**-0.81**	**-0.91**
	mys	β Integrin	**-0.47**	**-0.28**	**-0.56**	**-0.36**
	ltgβv	β Integrin	**-0.42**	-0.24	**-0.31**	**-0.31**
	scab	α Integrin	**-0.60**	**-0.43**	**-0.74**	**-0.80**
	ltgaPS4	α Integrin	**-1.37**	**-0.68**	**-0.79**	**-1.20**
	Dg	ECM	**-0.42**	-0.10	**-0.76**	**-0.53**
	trol	ECM	**-0.59**	-0.13	**-0.82**	**-0.40**
	LanA	ECM	-0.44	**-0.92**	**-0.56**	**-0.96**
	LanB2	ECM	-0.12	**-0.57**	**-0.48**	**-0.79**
	Ndg	ECM	-0.44	**-1.19**	**-0.63**	**-1.51**
Growth	*scrib*	Septate Junction	**-0.94**	**-0.51**	**-0.71**	**-0.87**
	ed	Adherens Junction	**-0.52**	-0.16	**-0.59**	-0.31
	crb	Hippo	**-0.74**	**-0.50**	**-0.61**	**-0.73**
	sdt	Hippo	**-0.88**	-0.33	-0.44	**-0.76**
	Pez	Hippo	**-0.84**	-0.32	**-1.00**	**-0.85**
	kibra	Hippo	-0.28	**-0.45**	**-1.42**	**-0.40**
	ex	Hippo	-0.33	**-0.68**	**-0.60**	**-0.95**
	wts	Hippo	**-0.64**	**-0.65**	-0.35	**-0.45**
	Socs36E	JAK/STAT	0.27	**0.90**	0.05	**0.60**
Cell Cycle	*CycE*	Replication	-0.15	**0.99**	0.03	**0.71**
	Cdk2	Replication	**0.89**	**0.78**	0.32	**1.00**
	E2f2	Replication	0.23	**0.56**	**0.46**	**0.58**
	Orc2	Replication	**0.99**	**0.87**	**0.64**	**0.75**
	PCNA	Replication	**1.08**	**0.85**	0.37	**0.60**
	Mcm5	Replication	**1.01**	**0.94**	**0.89**	**0.62**
	CycA	Replication/Mitosis	0.13	**0.59**	0.19	**0.52**
	CycB	Mitosis	0.08	**1.17**	-0.18	**0.78**
	Cdk1	Mitosis	**0.55**	**0.88**	0.21	**0.87**
	Cks30A	Mitosis	**1.27**	**0.79**	**1.09**	**0.63**

log2 FC
> 1.5
0
< -1.5

C

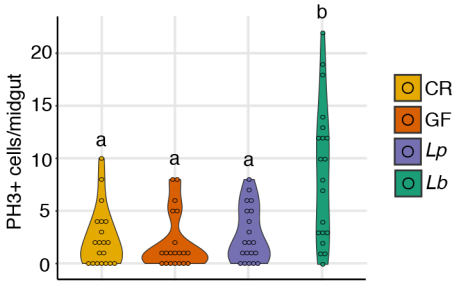

Figure 4. *L. brevis* disrupts expression of integrins in progenitor cells. **(A)** Biological process GO terms enriched in progenitors from $esg^{ts}/+$ colonized with *Lb* compared to GF. Enrichment score shown as bars and p values shown as dots. **(B)** Log2 fold change of genes involved in cell adhesion/polarity, Growth and Cell cycle affected by *Lb* in comparison to either GF or *Lp* colonization in $esg^{ts}/+$ and esg^{ts}/N^{RNAi} progenitors. Bolded values are those with a p value <0.05. **(C)** Number of PH3+ cells per $esg^{ts}/+$ midgut in gnotobiotic flies 8 days after colonization. Letters denote p<0.01 by pairwise Wilcoxon tests.

***L. brevis* colonization disrupts integrin localization independent of division.**

As integrins attach progenitor cells to the extracellular matrix, we asked what effects *Lb* has on progenitor compartment organization. In an initial experiment, we used transmission electron microscopy to visualize the posterior midguts of CR, and *Lb*-associated wild-type flies. CR flies had progenitor cells that were closely associated with the basal extracellular matrix (Fig. 5A). Mono-colonization with *Lb* appeared to disrupt intestinal organization, generating rounded progenitors that shifted apically relative to the extracellular matrix (Fig. 5B). These morphological changes were specific to progenitors, as no defects were apparent in the shape, or relative position of surrounding enterocytes. These observations prompted us to ask if *Lb* affected the distribution of integrins in progenitor cells. To answer this question, we determined the subcellular localization of the β-integrin, mys, in sagittal sections of control, GF wild-type intestines, or intestines that we associated with *Lb*. In GF flies, we detected a basal accumulation of mys in basally located progenitors (Fig. 5C). In contrast, and similar to our electron microscopy results, we found that *Lb* colonization caused progenitors to round up and adopt a more apical position within the epithelium (Fig. 5D). Furthermore, association with *Lb* had visible impacts on mys localization, characterized by discontinuous localization of basal mys (Fig. 5D, arrows), and apical enrichment of mys (Fig. 5D, arrowheads). To directly determine the effects of *Lb* on the

subcellular distribution of intestinal integrins, we developed an immunofluorescence-based assay that allowed us to quantify the apical/basal ratio of mys in intestinal progenitors (Suppl. Fig. 3A, B). Using this assay, we detected a basal enrichment of mys in progenitors of GF flies. Association with *Lb* caused a significant shift in the apical-basal distribution of mys, characterized by an increased proportion of mys along the apical edge of progenitors (Fig. 5F). As *Lb* stimulates stem cell proliferation, we asked if *Lb*-dependent effects on the subcellular distribution of mys is a downstream consequence of stem cell division. To test this hypothesis, we blocked division in the progenitors of *Lb*-associated flies by expressing the cell cycle inhibitor *dacapo* (*esg^{ts}/dap*) (Fig. 5G). Contrary to our expectations, we found that *Lb* continued to cause an increase in apical mys in progenitors that were incapable of cell division (Fig. 5F). Collectively, these data suggest that colonization of the intestine with *Lb* alters the apicobasal distribution of mys independent of ISC division.

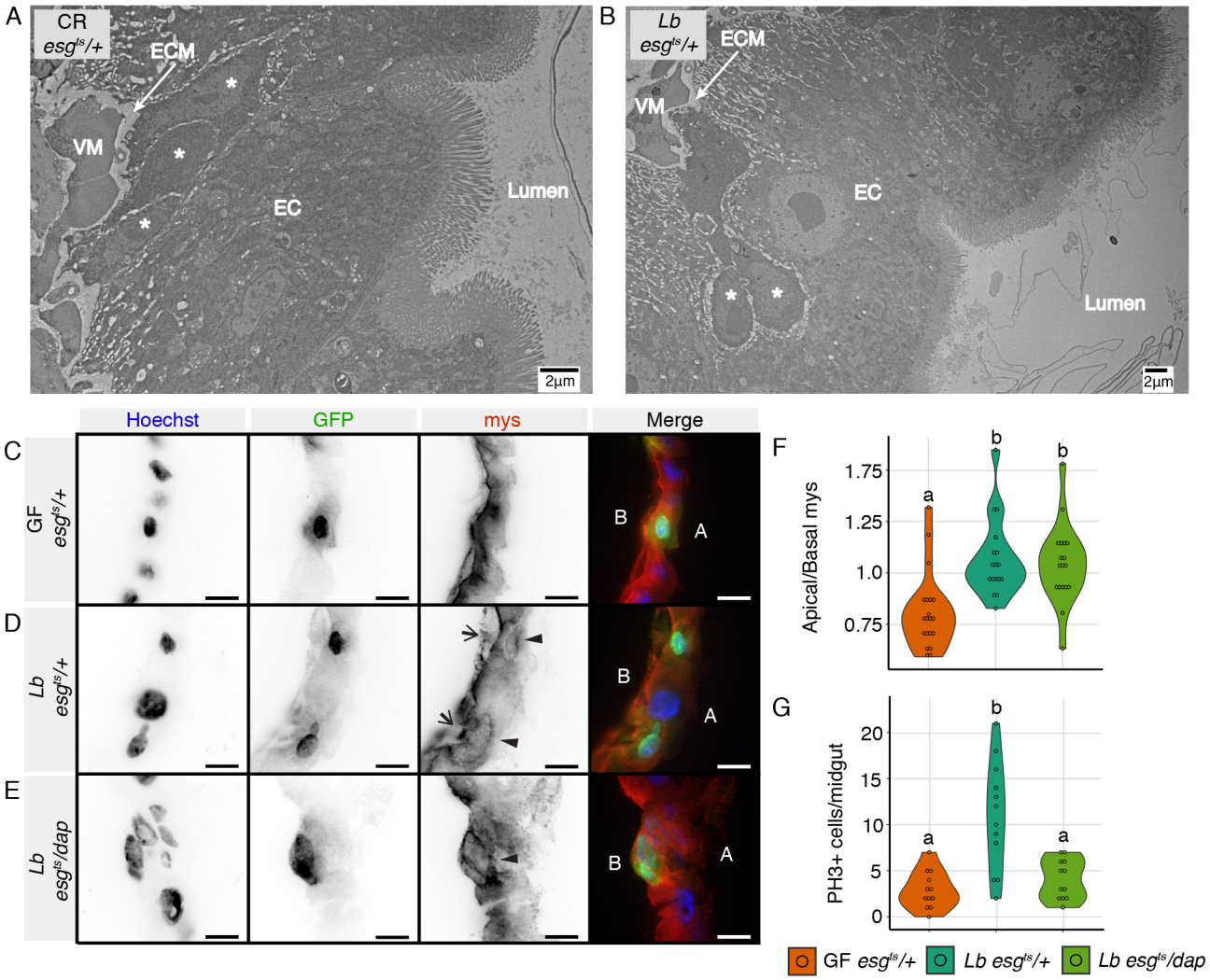

Figure 5. *L. brevis* colonization disrupts integrin localization independent of division. (A-B) TEM images of posterior midgut cross sections from *esg^{ts}/+* CR and *Lb* monoassociated flies. VM= visceral muscle, ECM= Extracellular matrix, EC= Enterocyte, *=progenitors. **(C-E)** Immunofluorescence images of posterior midgut sagittal sections from GF and *Lb* monoassociated *esg^{ts}/+* and *Lb* monoassociated *esg^{ts}/dap* flies after 8 days of transgene expression and bacterial colonization. Arrows = basal integrin disruption, arrowheads = apical integrin mislocalization, B = basal, A = apical. Scale bars = 10µm **(F)** Quantification of apical/basal mys intensity ratio from images captured from conditions in C-E. **(G)** Number of PH3+ cells per midgut of GF and *Lb* monoassociated *esg^{ts}/+* and *Lb* monoassociated *esg^{ts}/dap*

intestines after 8 days of transgene expression/bacterial colonization For F-G, letters denote p<0.01 by ANOVA followed by Tukey test.

L. brevis promotes symmetric stem cell expansion.

Since integrins modulate ISC divisions (Goulas et al., 2012), and *Lb* impacts the expression, and localization, of integrins we asked if *Lb* also affects the identity or organization of intestinal progenitors. To answer this question, we used Delta as a marker for ISCs to count the number of stem cells in the posterior midgut of $esg^{ts}/+$ flies that we raised under GF conditions, or in association with *Lb* (Fig. 6A-B). *Lb* association significantly increased the number of Delta+ ISCs compared to GF intestines (Fig. 6C), and increased the proportion of ISCs within *esg*+ progenitor populations (Fig. 6D), suggesting that association with *Lb* increases stem cell numbers within the epithelium at the expense of enteroblasts. To test this hypothesis, we used esg^{ts}*,UAS-CFP,Su(H)-GFP* flies to simultaneously visualize and quantify ISCs (CFP+/GFP-) and enteroblasts (CFP+/GFP+) in the intestines of CR, GF, and *Lb*-associated flies (Fig. 6E-G). With this line, both ISCs and enteroblasts are labelled with CFP under the control of the esg promoter, while enteroblasts are exclusively labelled with GFP under the control of the enteroblast specific marker Su(H). We found that the presence or absence of intestinal bacteria had no effect on the total number of enteroblasts within a given area (Fig. 6H). Instead, we detected microbe-specific effects on the relative amounts of ISCs and enteroblasts within the progenitor population. For example, the intestines of CR flies contained approximately equal numbers of ISCs and enteroblasts (Fig. 6I), and removal of the microbiome increased the proportion of enteroblasts at the expense of ISCs (Fig. 6I). Mono-association with *Lb* had the opposite effect. Here, we noticed a significant drop in enteroblast proportions within the progenitor population, indicating that *Lb* colonization expands the stem cell pool with a parallel loss of post-mitotic enteroblasts.

To determine if *Lb*-mediated shifts in ISC/enteroblast ratios is the result of changes in stem cell division type, we asked what effects *Lb* has on division symmetry. To quantify division symmetry, we identified progenitor pairs in the intestines of *esg^{ts},UAS-CFP,Su(H)-GFP* flies and categorized them into three subtypes; ISC/enteroblast (asymmetric division; arrows in 6E), enteroblast/enteroblast (symmetric division that leads to ISC loss; arrows in 6F), and ISC/ISC (symmetric division that lead to ISC clonal expansion; arrows in 6G). In agreement with previous reports (Jin et al., 2017; de Navascués et al., 2012; O'Brien et al., 2011), we found that roughly 70% of progenitor pairs were of the asymmetric ISC/EB class in CR intestines (Fig. 6J). We noted similar frequencies of asymmetric divisions in the posterior midguts, of GF, or *Lb*-associated flies (Fig. 6J), suggesting that the microbiota has minimal effects on the total frequency of asymmetric divisions. In contrast, examination of symmetric division subtypes uncovered substantial effects of the microbiota on the type of symmetric division within the posterior midgut. Both CR and GF intestines had low levels of symmetric divisions that yielded ISC/ISC pairs, at approximately 11.2% and 6.4%, respectively. However, association with *Lb* significantly increased the frequency of ISC/ISC pairs, accounting for 24.3% of all progenitor pairs, and roughly 80% of all symmetric pairs (Fig. 6J). Thus, association of the fly intestine with *Lb* significantly promotes the symmetric clonal expansion of stem cell populations.

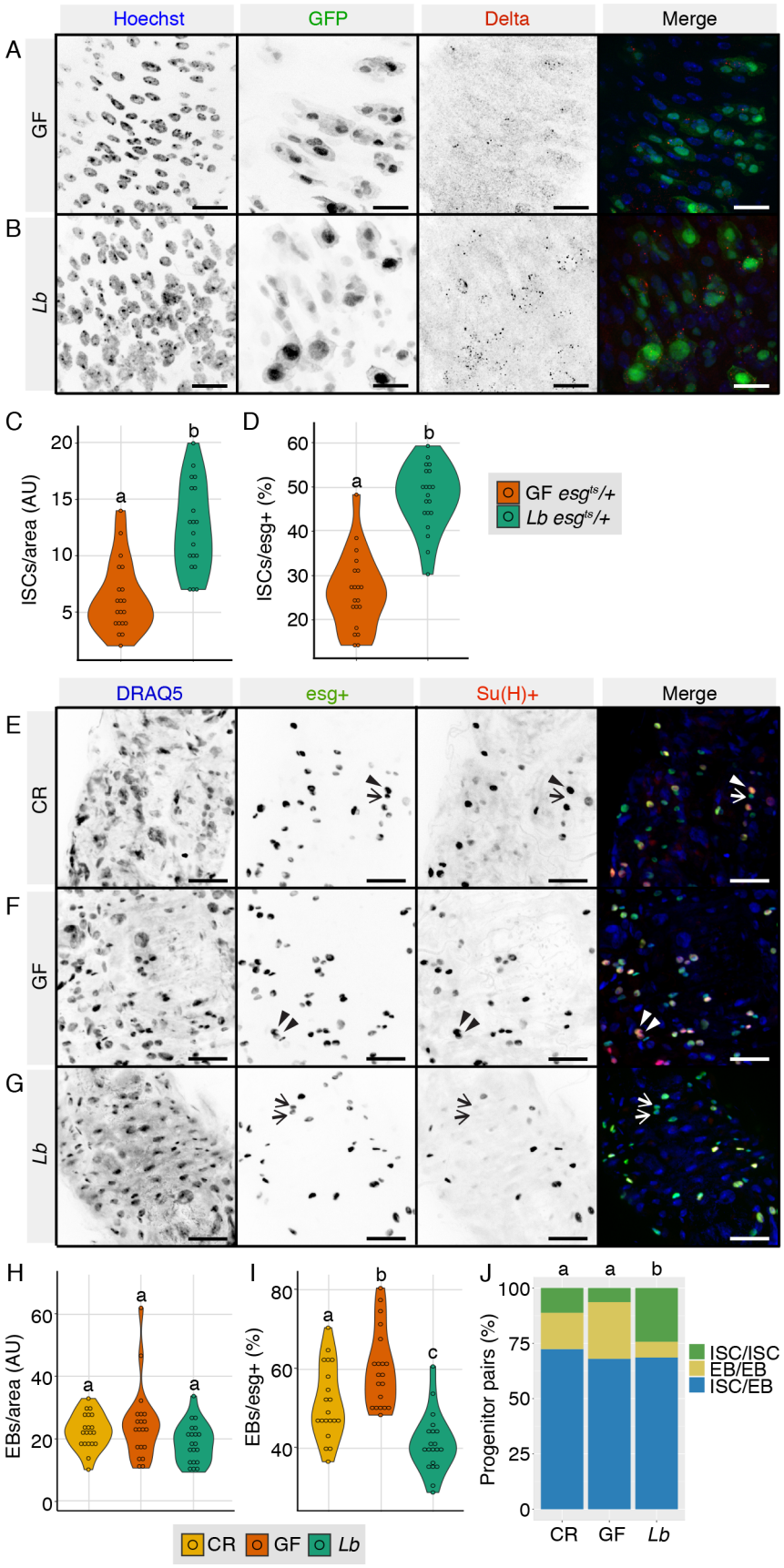

Figure 6. *L. brevis* promotes symmetric stem cell expansion. (A-B) Posterior midgut of *esg^{ts}/+* GF and *Lb* monoassociated flies where Delta (red) labels stem cells. Scale bars = 15μm **(C)** Number of Dl+ ISCs per area in posterior midguts of GF and Lb *esg^{ts}/+*. **(D)** Proportion of Dl+ ISCs within the esg+ progenitor population in GF and Lb *esg^{ts}/+*. For C and D, letters denote p<0.01 by ANOVA followed by Tukey test. **(E-G)** Posterior midgut of CR, GF or *Lb* monoassociated *esg^{ts},UAS-CFP,Su(H)-GFP* flies where DRAQ5 labels DNA, esg labels all progenitors and Su(H) labels enteroblasts. An asymmetric progenitor pair is shown in (E) with an ISC (arrow) and enteroblast (arrowhead). Arrowheads in (F) show symmetric enteroblast pair. Arrows in (G) show symmetric ISC pair. Scale bars = 50μm. **(H,I)** Number of total enteroblasts (EBs) per area and proportion of EBs within the esg+ progenitor population from CR, GF and *Lb* monoassociated *esg^{ts},UAS-CFP,Su(H)-GFP* intestines. Letters denote p<0.01 by ANOVA followed by Tukey test. **(J)** Proportion of ISC/ISC, EB/EB, and ISC/EB progenitor pairs in the posterior midgut of CR (n=134), GF (n=125) and *Lb* (n=140) monoassociated *esg^{ts},UAS-CFP,Su(H)-GFP* flies. Letters denote changed proportions of ISC/ISC pairs at p<0.01 by Chi-squared test.

DISCUSSION

Microbial factors promote growth and differentiation in the intestinal epithelium. Disrupted interactions between host cells and gut-resident microbial communities have detrimental health implications that include epithelial inflammation, and potentially oncogenic hyperplasia. To understand how gut bacteria cause progenitor cell dysplasia, we measured tumor formation and growth in adult *Drosophila* intestines that we mono-associated with common *Lactobacillus* symbionts. We chose *L. brevis* and *L. plantarum* for these studies, as they are known modifiers of *Drosophila* intestinal homeostasis (Combe et al., 2014; Fast et al., 2018; Jones et al., 2015; Lee et al., 2013; Storelli et al., 2011). Our study uncovered a feed-forward loop, where intestines that lack Notch activity in progenitors support host colonization by *L. brevis*, which promotes growth of *Notch*-deficient tumors. A similar feed-forward loop has recently been described using a BMP-deficient tumor model, where the microbiome promotes tumor growth and tumor intestines support bacterial growth (Zhou and Boutros, 2019). The commonalities between these two studies suggest that intestinal growth and differentiation is intimately linked to microbial growth. Mechanistically, we found that inactivation of Notch enhanced feeding, and suppressed antibacterial defenses in the intestine, phenotypes that support colonization by *Lb*. However, we hypothesize that additional mechanisms of Notch-dependant bacterial control exist. For example, Notch is required for the differentiation of copper cells in the *Drosophila* midgut (Wang *et al*., 2014), a cell population that attenuates bacterial growth by establishing a stomach-like region of low pH in the midgut (Li *et al*., 2016). Thus, we speculate that *Notch*-deficient intestines likely limit eradication of bacteria in the copper cell region.

In fractionation studies, we found that the cell wall of *L. brevis* promotes tumor growth, suggesting that bacterial recognition pathways may contribute to tumorigenesis in the host intestine. Consistent with this hypothesis, constitutive activation of the fly IMD pathway enhances the growth of Notch-

deficient tumors (Petkau *et al*., 2017). In addition, chronic inflammation in the intestine is a commonly associated risk factor for the development of colorectal cancer (Kim and Chang, 2014). Interestingly, *L. plantarum* does not promote tumor growth even though it grew to similar levels in the intestine as *L. brevis*. This raises the possibility that the *Lp* strain used in this study either fails to stimulate ISC growth, or that it actively inhibits ISC growth. In the future, it will be interesting to identify cell wall factors that are unique to *L. brevis*, and determine if these components differentially impact progenitor growth in the host.

To determine how *Lb* affects progenitor cell homeostasis, we characterized the transcriptional response of midgut progenitors inoculated with *Lb*. Consistent with a role in stem cell growth, we found that *Lb* activated cell cycle pathways in progenitors. In addition, we noticed significant effects of *Lb* on the expression and subcellular localization of integrins. Integrins are critical regulators of stem cell-niche interactions (Ellis and Tanentzapf, 2010; Fernandez-Minan et al., 2007; Marthiens et al., 2010; Toyoshima and Nishida, 2007), and mutations in integrin components impact stem cell division and maintenance (Goulas et al., 2012; Lin et al., 2013; Okumura et al., 2014; You et al., 2014). Typically, integrins accumulate at the basal margin of intestinal progenitors, and anchor interphase progenitors to the extracellular matrix. We found that *Lb* diminished the expression of key extracellular matrix proteins, integrin subunits with roles in ISC maintenance, and adaptor proteins that link integrins to the actin cytoskeleton. Furthermore, association with *Lb* led to an unexpected apicobasal redistribution of integrins in progenitor cells. The effects of *Lb* on integrin localization are not secondary to tumor development or cell cycle progression, as we observed similar phenotypes in wild-type intestines, and in progenitors that we arrested in G1. Furthermore, altered integrin gene expression patterns are not a general feature of host responses to *Lactobacillus* exposure, as association with *Lp* did not affect the expression of integrin pathway components. These data suggest that *Lb* has significant effects on the

expression and localization of mediators of integrin-dependent interactions between a stem cell and the niche.

In many tissues, including the fly intestine, integrins organize the stem cell division plane, by orienting the mitotic spindle. Progenitors mainly divide at angles greater than 20° to the basement membrane, leading to asymmetric divisions (Hu and Jasper, 2019; Ohlstein and Spradling, 2007), where daughter cells either remain in the niche and retain stemness, or exit the niche and differentiate. In contrast to other tissues, approximately 20% of divisions in the young adult intestine occur symmetrically (Hu and Jasper, 2019; Jin et al., 2017; O'Brien et al., 2011). In some cases, the switch from asymmetric to symmetric divisions facilitates beneficial responses to environmental fluctuations. Thus, rapid changes in nutrient availability, or ingestion of toxic doses of paraquat increase the frequency of symmetric divisions, allowing the host to tune intestinal physiology to the environment (Hu and Jasper, 2019; O'Brien *et al*., 2011). However, symmetric expansions of stem cell numbers is not a universal reply to intestinal damage. For example, infections with *Pseudomonas entomophila* or *Ecc15* accelerate the rate of stem cell divisions, but do not alter the frequency of symmetric divisions (Hu and Jasper, 2019; Jin *et al*., 2017), although it is unclear whether the subtype of symmetric divisions is altered by infection. In the context of aging, symmetric division frequency increases as the fly ages (Hu and Jasper, 2019). In this case, symmetric divisions are detrimental to host health and longevity, as genetic manipulations that diminish symmetric expansions improve gut barrier function, and extend lifespan (Hu and Jasper, 2019). Our study identifies *Lb* as an intestinal symbiont that causes symmetric ISC growth. The exact mechanism by which *Lb* promotes symmetric growth of stem cell numbers is unclear. However, the effects of *Lb* and integrin disruption on stem cell adhesion and polarity are reminiscent of the epithelial to mesenchymal transition (EMT), where epithelial cells disassemble cell junctions, rearrange their cytoskeleton and remodel cell-matrix adhesion to promote cell invasiveness and tumour metastasis (Kalluri and Weinberg,

2009). In mammals, Bone Morphogenic Protein (BMP) signaling plays a pivotal role in promoting the EMT (Mccormack et al., 2013; Zhang et al., 2016), and in *Drosophila*, BMPs produced by the surrounding tissue are important in stem cell niche maintenance, intestinal division symmetry and proliferation (Cai et al., 2019; Guo et al., 2013; Tian and Jiang, 2014; Tian et al., 2017; Zhou et al., 2015). Thus, it will be interesting to determine if *Lb* impacts BMP signaling in the intestinal epithelium.

In summary, we have identified a detrimental feed-forward loop, between *Notch*-deficient tumors, and symbiotic *L. brevis*. Mechanistically, we show that *L. brevis* disrupts integrin-mediated adhesion of stem cells to the niche and promotes symmetric stem cell divisions. In the presence of oncogenic mutations, *L. brevis* drives the clonal expansion of stem cells bearing oncogenic lesions, exacerbating tumourigenesis. Due to the evolutionary conservation of intestinal homeostatic regulators, we believe *Drosophila* will be a fruitful model to determine how gut-resident bacteria influence intestinal progenitor function.

ACKNOWLEDGEMENTS

We thank Dr. Bruce Edgar for providing us with the *esg*^{ts} and *Myo1A*^{ts} flies, Dr. Bruno Lemaitre for providing *imd* mutants and Dr. Lucy O'Brien for providing the *esg*^{ts}*,UAS-CFP,Su(H)-GFP* flies. We acknowledge microscopy support from Dr. Steven Ogg, Gregory Plummer and Woo Jung Cho at the Faculty of Medicine and Dentistry Imaging core. We acknowledge flow cytometry support from Dr. Aja Rieger at the Faculty of Medicine and Dentistry Flow Cytometry Core. We acknowledge cryo-sectioning support from Lynette Elder at the Alberta Diabetes Institute Histocore. The authors wish to thank Kin Chan at the Network Biology Collaborative Centre (nbcc.lunenfeld.ca) for the RNA-Seq service. Network Biology Collaborative Centre is a facility supported by Canada Foundation for Innovation, the Ontarian Government, and Genome Canada and Ontario Genomics (OGI-139). This work was supported by grants from the Canadian Institute of Health Research (Grant # PJT 159604). Anthony Galenza and David Fast have funding support through the National Science and Engineering Research Council scholarships. Meghan Ferguson has funding through Alberta Innovates Graduate Student Scholarships.

MATERIALS AND METHODS

Drosophila husbandry

Drosophila stocks and crosses were setup and maintained at 18-25°C on standard corn meal food (Nutri-Fly Bloomington formulation; Genesse Scientific) with a 12:12 light:dark cycle. All experimental flies were virgin female flies except when noted. Upon eclosion, flies were kept at 18°C then shifted to the appropriate temperature once 25-30 flies per vial was obtained. Germ free and mono-associated flies were generated as previously described (Fast et al., 2018). To generate germ free flies, freshly eclosed flies were fed autoclaved food with antibiotics (Ampicillin (100μg/mL), Neomycin (100μg/mL), Vancomycin (50μg/mL) and Metronidazole (100μg/mL)) for 5 days at 25°C. Conventionally reared controls were fed autoclaved food without antibiotics for 5 days at 25°C. To generate monoassociated animals, flies were made germ free as above then were fed 1mL OD_{600}=50 of *L. brevis* or *L. plantarum* resuspended in sterile 5% sucrose/PBS on a cotton plug overnight at 25°C. During this overnight feeding, CR and GF controls were fed sterile 5% sucrose/PBS without bacteria. The following morning, CR, *Lb* and *Lp* conditions were transferred to fresh autoclaved food at 29°C for the remainder of the experiment, while GF flies were maintained on autoclaved food with antibiotics. Sterility and mono-association were confirmed in each experimental vial by plating fly homogenate or fly food on MRS. Vials found to be contaminated were discarded from the experiment. Fly lines used in this study were: *w;esg-GAL4,tubGAL80^{ts},UAS-GFP* (*esg^{ts}*), *UAS-N^{RNAi}* (VDRC ID# 100002), w;*Myo1A-GAL4;tubGAL80^{ts},UAS-GFP (Myo1A^{ts})*, *imd*, *w^{1118}*, *UAS-ImdCA* (Petkau et al., 2017), *w;esg-GAL4,UAS-CFP, Su(H)-GFP;tubGal80^{ts} (esg^{ts},UAS-CFP,Su(H)-GFP)*.

Bacterial strains and growth conditions

L. brevis^{EF} (DDBJ/EMBL/GeneBank accession LPXV00000000) and *L. plantarum*^{KP} (DDBJ/EMBL/GenBank chromosome 1 CP013749 and plasmids 1-3 CP013750, CP013751, and CP013752) were both isolated from our *Drosophila* lab stocks and have been previously described (Petkau *et al*., 2016). Both bacteria were streaked out on MRS plates (BD; 288210) and aerobically grown at 29°C. Single colonies were picked for growth in MRS broth (Sigma; 69966) at 29°C (*L. brevis* for 2 days and *L. plantarum* for 1 day). To generate dead *L. brevis*, liquid culture was spun down, washed twice with sterile water then resuspended in sterile water before heating to 95°C for 30min. After heating, the killed bacteria was spun again and resuspended to 10mg/mL in sterile 5% yeast, 5% sucrose in PBS.

To extract the cell wall, *L. brevis* was heat killed as above, let cool on ice, then run through a French Press at 20,000 psi three times to lyse the bacterial cells. After lysis, any remaining whole cells were collected and discarded by two successive spins at 2000g. To collect the cell wall, the supernatant was spun at 10,000g for 30 minutes, washed twice with 1M NaCl and twice with sterile water before resuspending in sterile 5%yeast, 5% sucrose in PBS. Germ free flies were fed a 10mg/mL cell wall solution on filter paper disks on top of sterile food alongside 10mg/mL dead *L. brevis* and sterile 5% yeast, 5% sucrose PBS without any *L. brevis* extracts. Sterility of dead *Lb* and cell wall was confirmed by plating 100uL of extract on MRS.

Immunofluorescence

Intestines were dissected in PBS, fixed in 4% formaldehyde for 20 minutes then blocked overnight at 4°C in 5% normal goat serum (NGS), 1% bovine serum albumin (BSA), and 0.1% tween-20. Washes were done in blocking solution without NGS. Primary and secondary antibody incubations were done for 1 hour at room temperature in blocking buffer without NGS. For Delta and PH3 stain, we used a revised protocol where 8% formaldehyde was used to fix, washes were done in PBS with 0.2% TritonX-100 (PBST)

and blocked in PBST with 3% BSA. To prepare the intestinal sections, the posterior midgut was extracted, flash frozen on dry ice in frozen section compound (VWR 95057-838), sectioned to 10 μm and slides were stained using the same parameters as whole guts. Primary antibodies used: anti-prospero (1/100; Developmental Studies Hybridoma Bank(DSHB)), anti-mys (1/100; DSHB), anti-GFP (1/1000; Invitrogen), anti-phospho-histone3 (1/1000; Upstate), anti-Delta (1/100; DSHB). Secondary antibodies used: goat anti-mouse 568 (1/500; Invitrogen), goat anti-rabbit 488 (1/500; Invitrogen). DNA stains used: Hoechst (1/500; Molecular Probes), DRAQ5 (1/500; Invitrogen). Intestines were mounted on slides using Fluoromount (Sigma; F4680). For every experiment, images were obtained of the posterior midgut region (R4/5) of the intestine with a spinning disk confocal microscope (Quorum WaveFX). PH3+ cells were counted through the entire midgut. To determine the apical and basal mys intensity, we drew a line of 10 pixel width from the basal side to the apical (lumen side) side across GFP+ progenitor cells. We defined apical and basal progenitor cell borders as 50% of the maximum GFP intensity, as this GFP intensity coincides with the basal mys intensity peak. We determined the intensity of GFP and mys across the progenitors using the function plot profiles, copied these values into Excel and determined the apical and basal mys intensities. All image stacking, intensity and area calculations were done using Fiji software (Schindelin *et al*., 2019).

Intestinal progenitor cell isolation and RNA sequencing

Progenitor cell isolation by fluorescence activated cell sorting (FACS) was adapted from previously described protocols (Dutta *et al*., 2013). In brief, three biological replicates consisting of 100 fly guts per replicate with the malphigian tubules and crop removed were dissected into DEPC PBS and placed on ice. Guts were dissociated with 1mg/ml of elastase at 27°C with gentle shaking and periodic pipetting for 1hour. Progenitors were sorted based on GFP fluorescence and size with the BD FACSAria

III sorter. All small GFP positive cells were collected into DEPC PBS. Cells were pelleted at 1200g for 5 minutes and then resuspended in 500µl of Trizol. Samples were stored at -80°C until all samples were collected. RNA was isolated via a standard Trizol chloroform extraction and the RNA was sent on dry ice to the Lunenfeld-Tanenbaum Research Institute (Toronto, Canada) for library construction and sequencing. The sample quality was evaluated using Agilent Bioanalyzer 2100. TaKaRa SMART-Seq v4 Ultra Low Input RNA Kit for Sequencing was used to prepare full length cDNA. The quality and quantity of the purified cDNA was measure with Bioanalyzer and Qubit 2.0. Libraries were sequenced on the Illumina HiSeq3000 platform.

RNA Sequencing data processing and analysis

On average, we obtained 30 million reads per biological replicate. FASTQC was used to evaluate the quality of raw paired-end sequencing reads (http://www.bioinformatics.bbsrc.ac.uk/projects/fastqc, version 0.11.3). Adaptors and reads of less than 36 base pairs in length were trimmed from the raw reads using Trimmomatic (version 0.36) (Bolger *et al*., 2014). Reads were aligned to the *Drosophila* transcriptome- bdgp6 (https://ccb.jhu.edu/software/hisat2/index.shtml) with HISAT2 (version 2.1.0) (Kim *et al*., 2015). The resulting BAM files were converted to SAM flies using Samtools (version 1.8) (Li *et al*., 2009). The converted files were counted using Rsubread (version 1.24.2) (Liao and Smyth, 2019) and loaded into EdgeR (version 3.16.5) (Robinson *et al*., 2010). In EdgeR, genes with counts less than 1 count per million were filtered and libraries were normalized for size. Normalized libraries were used to call genes that were differentially expressed among treatments. Genes with P-value < 0.01 and FDR < 5% were defined as differentially expressed genes.

Principle component analysis was performed on normalized libraries using Factoextra (version 1.0.5) . Gene Ontology enRIchment anaLysis and visuaLizAtion tool (GORILLA) was used to examine Gene

Ontology (GO) term enrichment (Eden *et al*., 2009). Specifically, differentially expressed genes (defined above) were compared in a two-list unraked comparison to all genes output from edgeR as a background set. Redundant GO terms were removed.

Quantification of Bacterial CFUs

Five flies were randomly selected from a single vial of flies for each biological replicate and surface sterilized by washing in 10% bleach and 70% ethanol. Flies were then homogenized in MRS, serially diluted and 10μL of each dilution was plated on MRS. Colonies were counted from 10μL streaks that had 10-200 colonies and the CFU/fly calculated.

TEM

Intestines were dissected from virgin female flies that had been at 29°C for 8 days following germ free and bacterial association protocols. Posterior midguts were excised and fixed with 3% paraformaldehyde with 3% glutaraldehyde. Fixation, contrasting, sectioning, and visualization were performed at the Faculty of Medicine and Dentistry Imaging Core at the University of Alberta. Midgut sections were visualized with Hitachi H-7650 transmission electron microscope at 60Kv in high contrast mode.

Feeding assay

Each group of virgin female flies were shifted to 29°C for 5 days for transgene expression prior to feeding assay. Fly feeding behaviour was monitored using the FlyPAD for 1 hour as previously described (Itskov *et al*., 2014). Flies were starved on 1%(w/v) agar for 16hr at 29°C then placed in arenas with 3μL

of food made to be similar to the standard fly food. FlyPAD food was 400 calories/L made from sucrose, yeast extract and 1% agarose (80% carbohydrate and 20% protein).

Data visualization and Statistical analysis

All figures were constructed using R (version 3.3.1) via R studio (version 1.1.442) with easyggplot2 (version 1.0.0.9000), with the exception of GO term figures where ggplot2 (version 3.0.0) was used. Figures were assembled in Adobe Illustrator. All statistical analysis was performed in R.

Data availability

Gene expression data has been deposited to the NCBI GEO database accession GSE138555.

SUPPLEMENTARY FIGURES

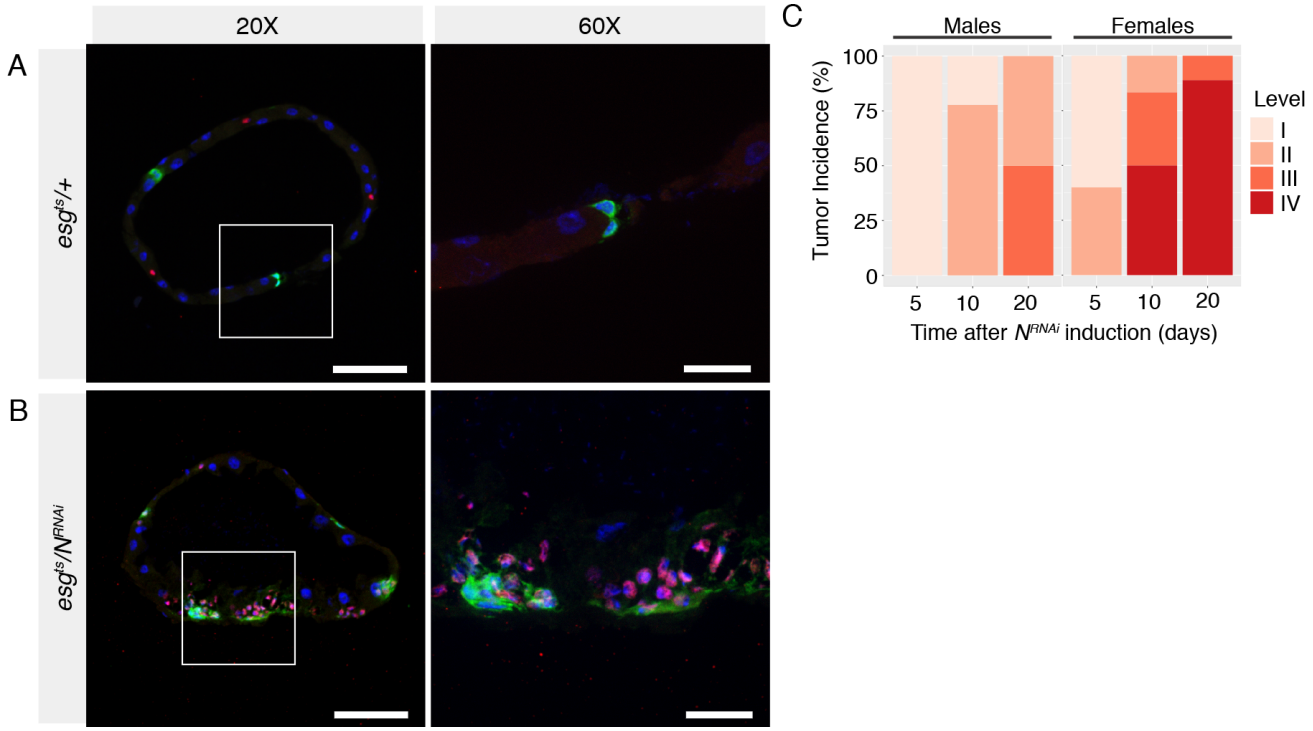

Supplementary Figure 1. Multilayered *Notch*-deficient tumors form in female *Drosophila* intestines. **(A)** Cross section of *esg^{ts}/+* posterior midgut and **(B)** cross section of *esg^{ts}/N^{RNAi}* showing multilayered tumors composed of enteroendocrine cells labelled by Prospero (red) and progenitors tagged with GFP. DNA labelled with Hoechst (blue). Scale bars: 20X = 50μm 60X = 15μm. **(C)** Incidence of tumors in male and female *esg^{ts}/N^{RNAi}* intestines 5, 10 and 20 days after *Notch* knockdown in intestinal progenitors.

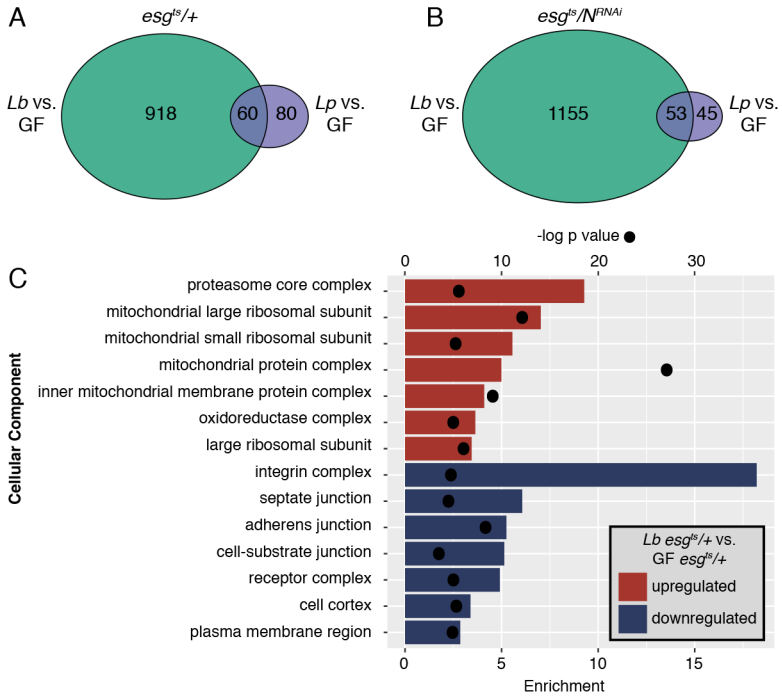

Supplementary Figure 2. Specific effect of *L. brevis* on integrin expression. (A-B) Number of significant genes (p<0.01, FDR<5%) differentially expressed in progenitors upon *Lb* or *Lp* mono-association in comparison with GF. **(A)** Comparisons from *esg^{ts}/+*. **(B)** Comparisons from *esg^{ts}/N^{RNAi}*. **(C)** Cellular component GO terms enriched in progenitors from *esg^{ts}/+* colonized with *Lb* compared to GF. Enrichment score shown as bars and p values shown as dots.

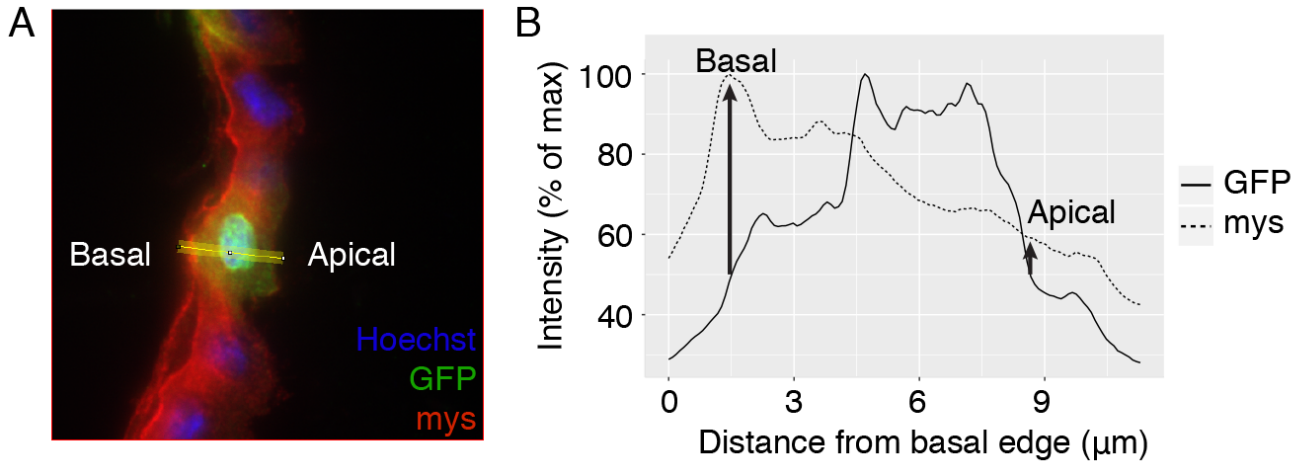

Supplementary Figure 3. Analysis of apicobasal integrin localization (A) Example image of intestinal cross section where intensities of mys (red) and GFP (progenitors) were measured along the yellow line from basal to apical edges of progenitors. **(B)** Plot showing the normalized intensities of GFP (solid line) and mys (dashed line) across the yellow line in (A). The basal and apical edges of progenitors were defined as 50% of the maximum GFP intensity and mys intensity was determined at each of these edges.

REFERENCES

Adair, K.L., Wilson, M., Bost, A., and Douglas, A.E. (2018). Microbial community assembly in wild populations of the fruit fly Drosophila melanogaster. ISME J.

Amcheslavsky, A., Jiag, J., and Ip, Y.T. (2009). Tissue Damage-Induced Intestinal Stem Cell Division in Drosophila. Stem Cell *4*, 49–61.

Biteau, B., and Jasper, H. (2011). EGF signaling regulates the proliferation of intestinal stem cells in Drosophila. Development *138*, 1045–1055.

Biteau, B., and Jasper, H. (2014). Slit/Robo Signaling Regulates Cell Fate Decisions in the Intestinal Stem Cell Lineage of Drosophila. Cell Rep. *7*, 1867–1875.

Blum, J.E., Fischer, C.N., Miles, J., and Handelsman, J. (2013). Frequent Replenishment Sustains the Beneficial Microbiome of Drosophila melanogaster. MBio *4*, 1–8.

Bolger, A.M., Lohse, M., and Usadel, B. (2014). Trimmomatic: a flexible trimmer for Illumina sequence data. Bioinformatics *30*, 2114–2120.

Broderick, N.A., and Lemaitre, B. (2012). Gut-associated microbes of Drosophila melanogaster. Gut Microbes *3*, 307–321.

Broderick, N.A., Buchon, N., and Lemaitre, B. (2014). Microbiota-Induced Changes in Drosophila melanogaster Host Gene Expression and Gut Morphology. MBio *5*, 1–13.

Buchon, N., Broderick, N.A., Chakrabarti, S., and Lemaitre, B. (2009a). Invasive and indigenous microbiota impact intestinal stem cell activity through multiple pathways in Drosophila. Genes Dev. *23*, 2333–2344.

Buchon, N., Broderick, N.A., Poidevin, M., Pradervand, S., and Lemaitre, B. (2009b). Drosophila Intestinal Response to Bacterial Infection: Activation of Host Defense and Stem Cell Proliferation. Cell Host Microbe *5*, 200–211.

Cai, X.T., Li, H., Safyan, A., Gawlik, J., Pyrowolakis, G., and Jasper, H. (2019). AWD regulates timed activation of BMP signaling in intestinal stem cells to maintain tissue homeostasis. Nat. Commun. *10*, 1–16.

Cheesman, S.E., Neal, J.T., Mittge, E., Seredick, B.M., and Guillemin, K. (2011). Epithelial cell proliferation in the developing zebra fish intestine is regulated by the Wnt pathway and microbial signaling via Myd88. PNAS *108*, 4570–4577.

Chen, A.J., Sayadian, A., Lowe, N., Lovegrove, H.E., and St Johnston, D. (2018). An alternative mode of epithelial polarity in the Drosophila midgut. PLoS Biol. *16*, 1–24.

Clark, R.I., Salazar, A., Pellegrini, M., William, W., Walker, D.W., Clark, R.I., Salazar, A., Yamada, R., Fitz-gibbon, S., Morselli, M., et al. (2015). Distinct Shifts in Microbiota Composition during Drosophila Aging Impair Intestinal Function and Drive Mortality. CellReports *12*, 1656–1667.

Combe, B.E., Defaye, A., Bozonnet, N., Puthier, D., Royet, J., and Leulier, F. (2014). Drosophila microbiota modulates host metabolic gene expression via IMD/NF-kB signaling. PLoS One *9*, 1–8.

Cordero, J.B., Stefanatos, R.K., Myant, K., Vidal, M., and Sansom, O.J. (2012). Non-autonomous crosstalk between the Jak/Stat and Egfr pathways mediates Apc1-driven intestinal stem cell hyperplasia in the Drosophila adult midgut. Development *139*, 4524–4535.

Crosnier, C., Vargesson, N., Gschmeissner, S., Ariza-McNaughton, L., Morrison, A., and Lewis, J. (2005). Delta-Notch signalling controls commitment to a secretory fate in the zebrafish intestine. Development *132*, 1093–1104.

Dutta, D., Xiang, J., and Edgar, B.A. (2013). RNA Expression Profiling from FACS-Isolated Cells of the Drosophila Intestine. Curr. Protoc. Stem Cell Biol. 2F.2.1-2F.2.12.

Eden, E., Navon, R., Steinfeld, I., Lipson, D., and Yakhini, Z. (2009). GOrilla: a tool for discovery and visualization of enriched GO terms in ranked gene lists. BMC Bioinformatics *10*, 1–7.

Ellis, S.J., and Tanentzapf, G. (2010). Integrin-mediated adhesion and stem-cell-niche interactions. Cell Tissue Res *339*, 121–130.

Fast, D., Duggal, A., and Foley, E. (2018). Monoassociation with Lactobacillus plantarum Disrupts Intestinal Homeostasis in Adult Drosophila melanogaster. MBio *9*, 1–16.

Fernandez-Minan, A., Martin-Bermudo, M.D., and Gonzalez-Reyes, A. (2007). Integrin Signaling Regulates Spindle Orientation in Drosophila to Preserve the Follicular-Epithelium Monolayer. Curr. Biol. *17*, 683–688.

Gagnière, J., Raisch, J., Veziant, J., Barnich, N., Bonnet, R., Buc, E., Bringer, M.A., Pezet, D., and Bonnet, M. (2016). Gut microbiota imbalance and colorectal cancer. World J. Gastroenterol. *22*, 501–518.

Goulas, S., Conder, R., and Knoblich, J.A. (2012). The Par Complex and Integrins Direct Asymmetric Cell Division in Adult Intestinal Stem Cells. Stem Cell *11*, 529–540.

Guo, Z., and Ohlstein, B. (2015). Bidirectional Notch signaling regulates Drosophila intestinal stem cell multipotency. Science (80-.). *350*, aab0988-1-aab0988-8.

Guo, L., Karpac, J., Tran, S.L., and Jasper, H. (2014). PGRP-SC2 Promotes Gut Immune Homeostasis to Limit Commensal Dysbiosis and Extend Lifespan. Cell *156*, 109–122.

Guo, Z., Driver, I., and Ohlstein, B. (2013). Injury-induced BMP signaling negatively regulates Drosophila midgut homeostasis. JCB *201*, 945–961.

Hu, D.J., and Jasper, H. (2019). Control of Intestinal Cell Fate by Dynamic Mitotic Spindle Repositioning Influences Epithelial Homeostasis and Longevity. CellReports *28*, 2807–2823.

Itskov, P.M., Moreira, J.-M., Vinnik, E., Lopes, G., Safarik, S., Dickinson, M.H., and Ribeiro, C. (2014). Automated monitoring and quantitative analysis of feeding behaviour in Drosophila. Nat. Commun. *5*, 4560.

Jiang, H., and Edgar, B.A. (2011). Intestinal stem cells in the adult Drosophila midgut. Exp. Cell Res. *317*,

2780–2788.

Jiang, H., Patel, P.H., Kohlmaier, A., Grenley, M.O., Donald, G., and Edgar, B.A. (2009). Cytokine/Jak/Stat signaling mediates regeneration and homeostasis in the Drosophila midgut. Cell *137*, 650–657.

Jin, Y., Patel, P.H., Kohlmaier, A., Pavlovic, B., Zhang, C., and Edgar, B.A. (2017). Intestinal Stem Cell Pool Regulation in Drosophila. Stem Cell Reports *8*, 1–9.

Jones, R.G., Li, X., Gray, P.D., Kuang, J., Clayton, F., Samowitz, W.S., Madison, B.B., Gumucio, D.L., and Kuwada, S.K. (2006). Conditional deletion of β 1 integrins in the intestinal epithelium causes a loss of Hedgehog expression, intestinal hyperplasia, and early postnatal lethality. JCB *175*, 505–514.

Jones, R.M., Desai, C., Darby, T.M., Luo, L., Wolfarth, A.A., Scharer, C.D., Ardita, C.S., Reedy, A.R., Keebaugh, E.S., and Neish, A.S. (2015). Lactobacilli Modulate Epithelial Cytoprotection through the Nrf2 Pathway. CellReports *12*, 1217–1225.

Kalluri, R., and Weinberg, R.A. (2009). The basics of epithelial-mesenchymal transition. J. Clin. Invest. *119*, 1420–1428.

Kim, E.R., and Chang, D.K. (2014). Colorectal cancer in inflammatory bowel disease : The risk , pathogenesis , prevention and diagnosis. World J. Gastroenterol. *20*, 9872–9881.

Kim, D., Langmead, B., and Salzberg, S.L. (2015). HISAT: a fast spliced aligner with low memory requirements. Nat. Methods *12*.

Koyle, M.L., Veloz, M., Judd, A.M., Wong, A.C.-N., Newell, P.D., Douglas, A.E., and Chaston, J.M. (2016). Rearing the Fruit Fly Drosophila melanogaster Under Axenic and Gnotobiotic Conditions. J. Vis. Exp. 1–8.

Lee, K.A., Kim, S.H., Kim, E.K., Ha, E.M., You, H., Kim, B., Kim, M.J., Kwon, Y., Ryu, J.H., and Lee, W.J. (2013). Bacterial-derived uracil as a modulator of mucosal immunity and gut-microbe homeostasis in

drosophila. Cell *153*, 797–811.

Li, H., Handsaker, B., Wysoker, A., Fennell, T., Ruan, J., Homer, N., Marth, G., Abecasis, G., Durbin, R., and Subgroup, 1000 Genome Project Data Processing (2009). The Sequence Alignment/Map format and SAMtools. Bioinformatics *25*, 2078–2079.

Li, H., Qi, Y., and Jasper, H. (2016). Preventing Age-Related Decline of Gut Compartmentalization Limits Microbiota Dysbiosis and Extends Lifespan. Cell Host Microbe *19*, 240–253.

Li, Y., Kundu, P., Seow, S.W., Matos, C.T. De, Aronsson, L., Pettersson, S., and Greicius, G. (2012). Gut microbiota accelerate tumor growth via c-jun and STAT3 phosphorylation in APCMin/+ mice. Carcinogenesis *33*, 1231–1238.

Liao, Y., and Smyth, G.K. (2019). The R package Rsubread is easier , faster , cheaper and better for alignment and quantification of RNA sequencing reads. *47*.

Lin, G., Zhang, X., Ren, J., Pang, Z., Wang, C., Xu, N., and Xi, R. (2013). Integrin signaling is required for maintenance and proliferation of intestinal stem cells in Drosophila. Dev. Biol. *377*, 177–187.

Marthiens, V., Kazanis, I., Moss, L., Long, K., and Ffrench-Constant, C. (2010). Adhesion molecules in the stem cell niche – more than just staying in shape? J. Cell Sci. *123*, 1613–1622.

Martin, J.L., Sanders, E.N., Moreno-roman, P., Koyama, L.A.J., Balachandra, S., Du, X., and O'Brien, L.E. (2018). Long-term live imaging of the Drosophila adult midgut reveals real-time dynamics of division, differentiation and loss. Elife *7*, 1–33.

Mccormack, N., Molloy, E.L., and O'Dea, S. (2013). Bone morphogenetic proteins enhance an epithelial-mesenchymal transition in normal airway epithelial cells during restitution of a disrupted epithelium. Respir. Res. *14*, 1–12.

Micchelli, C.A., and Perrimon, N. (2006). Evidence that stem cells reside in the adult Drosophila midgut epithelium. Nature *439*, 475–479.

Miguel-Aliaga, I., Jasper, H., and Lemaitre, B. (2018). Anatomy and Physiology of the Digestive Tract of Drosophila melanogaster. Genetics *210*, 357–396.

Morrison, S.J., and Spradling, A.C. (2008). Stem Cells and Niches: Mechanisms That Promote Stem Cell Maintenance throughout Life. Cell *132*, 598–611.

de Navascués, J., Perdigoto, C.N., Bian, Y., Schneider, M.H., Bardin, A.J., Martínez-Arias, A., and Simons, B.D. (2012). *Drosophila* midgut homeostasis involves neutral competition between symmetrically dividing intestinal stem cells. EMBO J. *31*, 2473–2485.

O'Brien, L.E., Soliman, S.S., Li, X., and Bilder, D. (2011). Altered Modes of Stem Cell Division Drive Adaptive Intestinal Growth. Cell *147*, 603–614.

Ohlstein, B., and Spradling, A. (2006). The adult Drosophila posterior midgut is maintained by pluripotent stem cells. Nature *439*, 470–474.

Ohlstein, B., and Spradling, A. (2007). Multipotent Drosophila Intestinal Stem Cells Specify Daughter Cell Fates by Differential Notch Signaling. Science (80-.). *315*, 988–993.

Okumura, T., Takeda, K., Taniguchi, K., and Adachi-yamada, T. (2014). Bv Integrin Inhibits Chronic and High Level Activation of JNK to Repress Senescence Phenotypes in Drosophila Adult Midgut. PLoS One *9*, 1–14.

Pais, S., Valente, R.S., Sporniak, M., and Teixeira, L. (2018). Drosophila melanogaster establishes a species- specific mutualistic interaction with stable gut-colonizing bacteria. PLoS Biol. *16*, 1–45.

Patel, P.H., Dutta, D., and Edgar, B. a (2015). Niche appropriation by Drosophila intestinal stem cell tumours. Nat. Cell Biol. *17*, 1182–1192.

Petkau, K., Fast, D., Duggal, A., and Foley, E. (2016). Comparative evaluation of the genomes of three common Drosophila-associated bacteria. Biol. Open *5*, 1305–1316.

Petkau, K., Ferguson, M., Guntermann, S., and Foley, E. (2017). Constitutive Immune Activity Promotes

Tumorigenesis in Drosophila Intestinal Progenitor Cells. CellReports *20*, 1784–1793.

Qiao, L., and Wong, B.C.Y. (2009). Role of notch signaling in colorectal cancer. Carcinogenesis *30*, 1979–1986.

Robinson, M.D., Mccarthy, D.J., and Smyth, G.K. (2010). edgeR: a Bioconductor package for differential expression analysis of digital gene expression data. Bioinformatics *26*, 139–140.

Schindelin, J., Arganda-carreras, I., Frise, E., Kaynig, V., Longair, M., Pietzsch, T., Preibisch, S., Rueden, C., Saalfeld, S., Schmid, B., et al. (2019). Fiji: an open-source platform for biological-image analysis. Nat. Methods *9*, 676–682.

Shaw, R.L., Kohlmaier, A., Polesello, C., Veelken, C., Edgar, B.A., and Tapon, N. (2010). The Hippo pathway regulates intestinal stem cell proliferation during Drosophila adult midgut regeneration. Development *137*, 4147–4158.

Siudeja, K., Nassari, S., Gervais, L., Skorski, P., Lameiras, S., Stolfa, D., Zande, M., Bernard, V., Frio, T.R., and Bardin, A.J. (2015). Frequent Somatic Mutation in Adult Intestinal Stem Cells Drives Neoplasia and Genetic Mosaicism during Aging. Cell Stem Cell *17*, 663–674.

Storelli, G., Defaye, A., Erkosar, B., Hols, P., Royet, J., and Leulier, F. (2011). Lactobacillus plantarum promotes drosophila systemic growth by modulating hormonal signals through TOR-dependent nutrient sensing. Cell Metab. *14*, 403–414.

Takashima, S., and Hartenstein, V. (2012). Genetic control of intestinal stem cell specification and development: a comparitive view. Stem Cell Rev. *8*, 597–608.

Tian, A., and Jiang, J. (2014). Intestinal epithelium-derived BMP controls stem cell self-renewal in Drosophila adult midgut. Elife *3*, 1–23.

Tian, A., Wang, B., and Jiang, J. (2017). Injury-stimulated and self-restrained BMP signaling dynamically regulates stem cell pool size during Drosophila midgut regeneration. PNAS E2699–E2708.

Toyoshima, F., and Nishida, E. (2007). Spindle Orientation in Animal Cell Mitosis: Roles of Integrin in the Control of Spindle Axis. J. Cell. Physiol. 407–411.

Wang, C., Guo, X., and Xi, R. (2014). EGFR and Notch signaling respectively regulate proliferative activity and multiple cell lineage differentiation of Drosophila gastric stem cells. Cell Res. *24*, 610–627.

You, J., Zhang, Y., Li, Z., Lou, Z., Jin, L., and Lin, X. (2014). Drosophila Perlecan Regulates Intestinal Stem Cell Activity via Cell-Matrix Attachment. Stem Cell Reports *2*, 761–769.

Zackular, J.P., Baxter, N.T., Iverson, K.D., Sadler, W.D., Petrosino, J.F., Chen, G.Y., and Schloss, P.D. (2013). The Gut Microbiome Modulates Colon Tumorigenesis. MBio *4*, 1–9.

Zeller, G., Tap, J., Voigt, A.Y., Sunagawa, S., Kultima, J.R., Costea, P.I., Amiot, A., Böhm, J., Brunetti, F., Habermann, N., et al. (2014). Potential of fecal microbiota for early-stage detection of colorectal cancer. Mol. Syst. Biol. *10*, 766.

Zeng, X., and Hou, S.X. (2015). Enteroendocrine cells are generated from stem cells through a distinct progenitor in the adult Drosophila posterior midgut. Development *142*, 644–653.

Zhang, L., Ye, Y., Long, X., Xiao, P., Ren, X., and Yu, J. (2016). BMP signaling and its paradoxical effects in tumorigenesis and dissemination. Oncotarget *7*.

Zhou, J., and Boutros, M. (2019). JNK-dependent intestinal barrier failure disrupts host-microbe homeostasis during tumorigenesis. BioRxiv. http://dx.doi.org/10.1101/719468

Zhou, J., Florescu, S., Boettcher, A., Luo, L., Dutta, D., Kerr, G., Cai, Y., Edgar, B.A., and Boutros, M. (2015). Dpp/Gbb signaling is required for normal intestinal regeneration during infection. Dev. Biol. *399*, 189–203.